Cell

Resource

Paper-Based Synthetic Gene Networks

Keith Pardee,[1,2] Alexander A. Green,[1,2] Tom Ferrante,[1] D. Ewen Cameron,[2,3] Ajay DaleyKeyser,[1] Peng Yin,[1] and James J. Collins[1,2,3,*]

[1]Wyss Institute for Biological Inspired Engineering, Harvard University, Boston, MA 02115, USA
[2]Department of Biomedical Engineering and Center of Synthetic Biology, Boston University, Boston, MA 02215, USA
[3]Howard Hughes Medical Institute, Chevy Chase, MD 20815, USA
*Correspondence: jcollins@bu.edu
http://dx.doi.org/10.1016/j.cell.2014.10.004

SUMMARY

Synthetic gene networks have wide-ranging uses in reprogramming and rewiring organisms. To date, there has not been a way to harness the vast potential of these networks beyond the constraints of a laboratory or in vivo environment. Here, we present an in vitro paper-based platform that provides an alternate, versatile venue for synthetic biologists to operate and a much-needed medium for the safe deployment of engineered gene circuits beyond the lab. Commercially available cell-free systems are freeze dried onto paper, enabling the inexpensive, sterile, and abiotic distribution of synthetic-biology-based technologies for the clinic, global health, industry, research, and education. For field use, we create circuits with colorimetric outputs for detection by eye and fabricate a low-cost, electronic optical interface. We demonstrate this technology with small-molecule and RNA actuation of genetic switches, rapid prototyping of complex gene circuits, and programmable in vitro diagnostics, including glucose sensors and strain-specific Ebola virus sensors.

INTRODUCTION

The field of synthetic biology aims to re-engineer the molecular components of the cell to harness the power of biology. In doing so, synthetic biologists have created whole-cell biosensors (Kobayashi et al., 2004; Kotula et al., 2014), synthetic probiotics, new sources of drugs (Fossati et al., 2014), green energy, (Torella et al., 2013) and chemistry (Zhang et al., 2012; Martin et al., 2003). At the heart of many of these cellular technologies are synthetic gene networks (Elowitz and Leibler, 2000; Gardner et al., 2000), which are decision-based circuits often composed of a sensor element followed by a transducer that regulates a measureable output (Figure 1A). With sequence-specific sensing of nucleic acids and small-molecule recognition, these engineered logic and output elements hold great potential for broad biotechnology and medical applications. However, the application of cell-based synthetic gene networks outside of the laboratory has been restricted by concerns of biosafety and the practicality of the cellular host.

Earlier studies in the area of in vitro synthetic biology and cell-free systems have made important contributions to our understanding of fundamental molecular biology and biochemistry and, more recently, in the study of molecular switch dynamics and complex gene circuits (Hong et al., 2014; Karzbrun et al., 2014; Sun et al., 2014; Takahashi et al., 2014). These efforts, however, have focused on solution-phase reactions using fresh from frozen cell-free systems and often in liposomes with the goal of assembling artificial cells (Kuruma et al., 2009; Kobori et al., 2013). These solution-phase reactions are not stable or practical for handling outside of the lab and therefore miss the opportunity to leverage the abiotic and sterile nature of these systems.

Here, we report a method for embedding cell-free synthetic gene networks onto paper and other materials for in vitro applications in the clinic, global health, industry, research, and education. This is achieved by freeze drying cell-free systems into paper and other porous substrates to create materials with the fundamental transcription and translation properties of a cell but that are sterile and abiotic (Figure 1A). Stable at room temperature, these embedded materials are readily stored, distributed, and can be activated by simply adding water. We begin by demonstrating the successful operation of synthetic networks in this alternative medium for biomolecular reactions and then move on to show rapid screening of gene constructs and application of the paper-based platform for programmable in vitro diagnostics, including strain-specific Ebola sensors.

RESULTS

Development of Paper-Based Technology

To begin, we tested to see whether the enzyme activity required for transcription and translation could be reconstituted from freeze-dried cell-free expression systems, which normally require storage at −80°C. The commercially available PT7 expression system, which is assembled from ribosomes and 35 purified bacterial proteins (Shimizu et al., 2001; Shimizu and Ueda, 2010), was freeze dried to form a pellet, reconstituted in water, and then used to transcribe and translate a constitutive *GFP* expression cassette. Remarkably, the freeze-dried and reconstituted PT7 solution-phase reactions showed activity comparable to the fresh from frozen PT7 reactions (Figure 1B). This approach was then extended to systems with greater molecular complexity based on whole-cell extracts. Using expression constructs dependent on either *E. coli* RNA polymerase (RNAP; S30) or T7

RNAP (S30 T7), constitutive expression of GFP was supported in small, solution-phase reactions started from freeze-dried pellets (Figures S1A and S1B available online). Importantly, these freeze-dried pellets are stable over time, with PT7 transcription and translation activity remaining after a year of room temperature storage (Figure 1C).

Although freeze-dried preparations offer great potential for the storage of poised synthetic biology tools, the handling of solution-phase reactions is awkward for applications outside of the lab. To address this, we embedded the cell-free systems and synthetic gene networks onto paper and other porous materials (Figure 1A). Previously used in measuring pH and more recently in chemistry-based diagnostics (Martinez et al., 2007), we speculated that paper could also serve as high-capillary-action matrix to hold small-volume molecular and biochemical reactions. To begin, we tested whether simple cell-free expression could be supported while embedded in the cellulose matrix of paper.

Small 2 mm filter paper discs were freeze dried with bacterial cell-free systems containing either *E. coli* (S30) or T7 RNAPs (S30 T7, PT7) and a corresponding *GFP* expression plasmid (Figure 1D). For all experiments, unless otherwise specified, the gene construct or network was freeze dried as a DNA copy into paper discs, along with the appropriate cell-free system (Figure S1G). After being freeze dried and rehydrated, these paper-based reactions yielded consistent GFP fluorescence under the regulation of either RNAP. Fluorescence imaging of the paper discs confirm GFP expression, and reactions were monitored by placing the paper discs at the bottom of black, clear-bottom 384-well plates for incubation in a 37°C plate reader (Figure 1E).

Synthetic Gene Networks

Next, we tested inducible expression systems to determine whether more complex synthetic gene networks could be supported by the freeze-dried, paper-based reactions (Figure 1A). We started with tetO-regulated expression. Regulation of this system is mediated by the Tet repressor (TetR) that binds to the tetO promoter, preventing transcription (Figure 1F; Lutz and Bujard, 1997). Such regulation performed in vitro required that constitutive *TetR* expression also be encoded into the synthetic gene network. Expression is then induced by addition of the tetracycline analog anhydrotetracycline (aTc), which disrupts TetR binding to the promoter, allowing transcription of the regulated gene.

Freeze-dried discs were prepared with a cell-free system containing S30 *E. coli* cell extract, pretranslated TetR, and the network elements encoding the constitutive expression of *TetR* and tetO-regulated *GFP* or *mCherry*. Varying only the presence of aTc, discs were rehydrated and incubated at 37°C. The aTc-induced discs yielded expression of GFP and mCherry at 5- and 32-fold, respectively (Figures 1G, S1C, and S1D). To optimize performance, we found that regulatory control from the tetO promoter could be tightened if cell extracts were supplemented, prior to freeze drying, with TetR to control promoter leakage prior to the expression of the encoded *TetR* (Figures S1E and S1F). This successful TetR augmentation of cell-free systems prior to freeze drying suggests that protein doping may be a useful way to tailor and enhance the regulatory and enzymatic environment of cell-free applications.

An important trend for synthetic biology is the use of RNA-actuated gene circuits (Callura et al., 2012). Unlike circuits based on small-molecule-based regulation, which are limited by the number of available unique recognition domains, RNA-based switches can be rationally programmed to recognize sequence-specific triggers and accordingly have the potential to offer essentially unlimited design and signaling space (Isaacs et al., 2004; Callura et al., 2010; Lucks et al., 2011; Mutalik et al., 2012). Here, we test a new generation of riboregulators in an in vitro demonstration of toehold switches (Green et al., 2014 [this issue of *Cell*]). These robust biomolecular switches provide tight translational regulation over transcripts and exhibit excellent orthogonality. Moreover, as we will demonstrate, by controlling the expression of alternative RNA polymerases (e.g., T3 RNAP), toehold switches can also trigger the synthesis of additional switch RNAs, enabling cascades and more sophisticated synthetic circuits.

The rational programmability of toehold switches comes from their design (Figure 2A). Riboregulators are composed of two cognate RNAs: a transducer RNA that encodes the output signal of the system (e.g., a GFP mRNA) and a trigger RNA that modulates the output signal. Conventional riboregulators have historically repressed translation by sequestering the ribosomal binding site (RBS) of the transducer RNA within a hairpin. This hairpin is unwound upon binding of a cognate trigger RNA, exposing the RBS and enabling translation of the downstream protein. However, this design restricts the potential trigger RNAs to those that contain RBS sequences. Toehold switches have removed this constraint by moving the RBS to a loop region of the hairpin, leaving the trigger RNA binding site free to adopt virtually any sequence. The transducer or "switch" RNA of toehold switches also contains a single-stranded domain known as a toehold at its 5′ end. This toehold domain, first developed in in vitro molecular programming studies (Yurke et al., 2000), provides the initial reaction site for binding between the trigger and switch RNAs and greatly improves the ON/OFF ratio of the switches.

We began by demonstrating the regulation of GFP expression under the control of eight different toehold switches on paper. Experiments were performed by freeze drying the recombinant PT7 expression system onto paper discs, along with linear DNA encoding specific switch RNAs. The paper discs were rehydrated with or without the complementary RNA trigger 24 hr after drying and then incubated at 37°C in humid chamber for 2 hr. As expected, discs that received the trigger RNA exhibited strong GFP expression, whereas control discs exhibited little, if any, expression (Figure 2B). Toehold switch and trigger RNAs can also be directly applied to the paper at the appropriate times or synthesized from DNA on the paper. By freeze drying the paper with pretranscribed toehold switch RNA, we were able to detect positive reactions 6 to 8 min earlier than having the RNAs transcribed in place (data not shown). However, due to the greater stability of DNA, we chose to freeze dry all paper reactions with DNA copies of the respective toehold switches.

Parallel experiments were done to measure reaction kinetics. We found that, within 90 min of 37°C incubation, the maximum ON/OFF ratios ranged between 10- and 140-fold (Figure 2C), with signal detection in as little as 20 min (Figure S2A). Maximum expression rates occurred between 60 and 120 min, and the

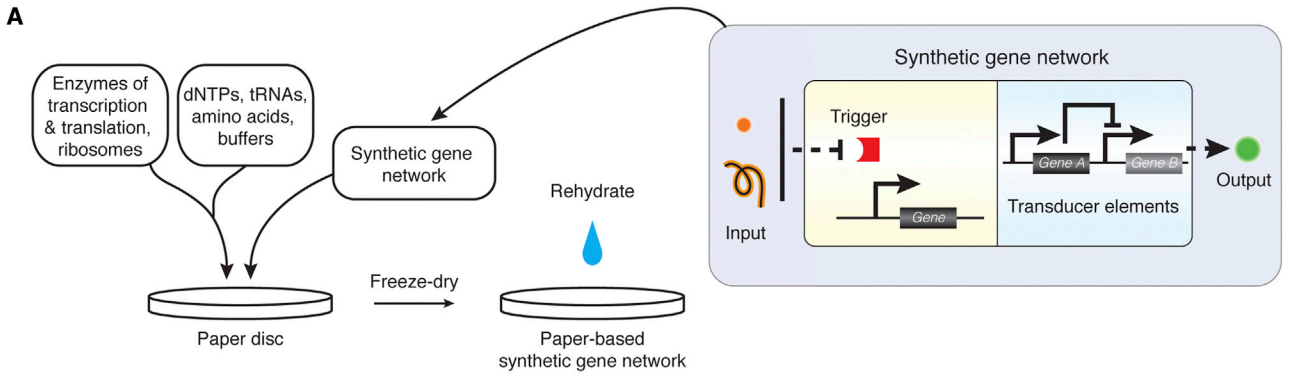

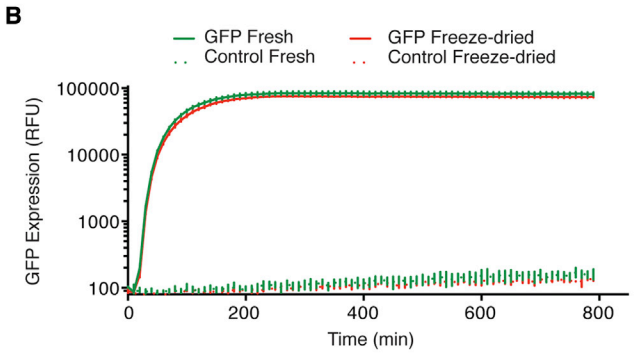

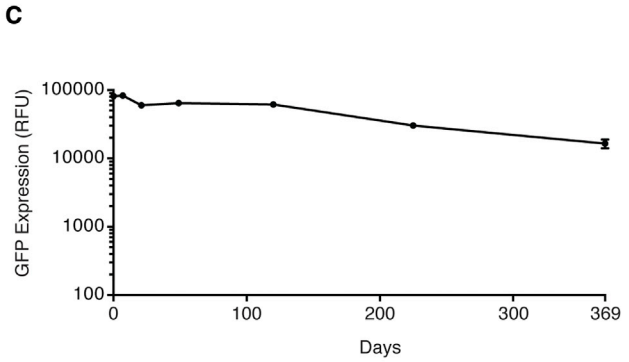

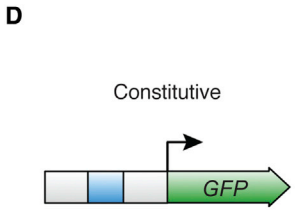

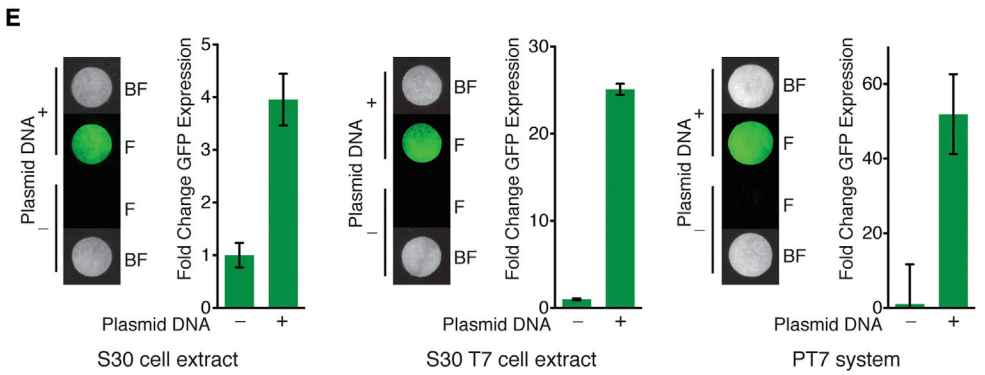

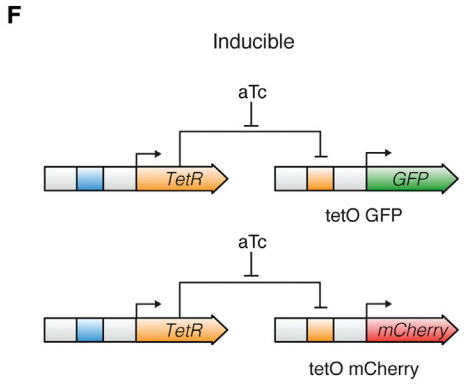

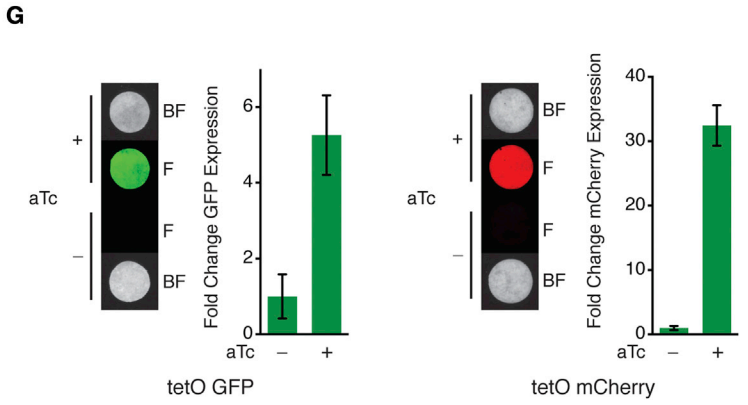

(legend on next page)

reaction output generally reached a plateau by 200 min. Taking advantage of the nuclease-free nature of the PT7 recombinant system, we titrated RNA directly into the reactions and found a linear response to RNA concentration between low nanomolar and low micromolar concentrations (Figure S2B). We continued to use purified trigger RNAs so that we could control the concentration and chose 5 μM trigger RNA to maximize response in demonstration reactions. It is also of note that switch behavior in freeze-dried lysates replicates that of toehold switches in vivo in *E. coli* (Figure S2C; Green et al., 2014). Importantly, the clear target-dependent induction of the toehold switches in the RNA-rich environment of *E. coli* helps to demonstrate sequence specificity of these RNA components.

Whole-cell extracts and cellulose fibers exhibit an inherent autofluorescence around the emission spectrum of GFP (Schmidt, 2010), so we also constructed gene circuits to contain output fluorescent proteins with alternate emission spectra for both paper and quartz microfiber discs (Figures 2D and S2D). With these distinct outputs, a single paper disc can also be used to host multiple toehold switches, each capable of individual activation and measurement (Figure S2E). We also successfully tested toehold switches in S30 T7 *E. coli* cell extracts, a lower cost alternative, using circularized DNA plasmid as a template for both toehold switch and trigger RNAs (data not shown).

By arraying the paper discs into a 384-well plate, multiplexed reactions can be easily quantified and measured over time. We tested the orthogonality of the toehold switches by combining each of the eight toehold hairpins against each of the trigger RNAs. As seen in Figure 2E, activation of the toehold switches was essentially limited to the diagonal, with only one weak off-target interaction between switch E and trigger H (Figures 2E, 2F, S2G, and S2H). Despite not being explicitly designed to be orthogonal to one another, significant orthogonality was also reflected in the specific activation demonstrated above in the in vivo milieu of bacteria cells (Figure S2C). This arrayed approach also underscores another important advantage of our in vitro paper-based system, namely, the rapidity with which it can used to rationally design and test synthetic constructs. To collect similar data in vivo would require 81 separate transformations, overnight cultures on plates, and subsequent culturing in multiwell plates and could take several days. Using in vitro paper-based reactions, this experiment took under 90 min to set up, and, upon incubation, signals from activated switches were detected in as little as 20 min (Figure S2H).

Enabling Technologies

In keeping with our goal of making synthetic biology-based tools widely available outside of the laboratory, we designed our paper-based system to generate a colorimetric output visible to the naked eye. To do so, we replaced GFP with the enzyme β-galactosidase (LacZ) to create a synthetic gene network that generates a dramatic enzyme-mediated color change in response to conditional inputs (Figure 3A). LacZ cleaves the yellow substrate, chlorophenol red-β-D-galactopyranoside, embedded into the freeze-dried paper discs, to produce a purple chlorophenol red product that is visible to the naked eye and can be measured on standard plate readers by monitoring the absorbance at 570 nm.

As with fluorescent outputs from the GFP toehold switches, each triggered LacZ switch produces a unique switch-dependent response, with maximum expression rates occurring between 50 and 120 min (Figures 3B, 3C, and S3A). Some toehold switches rapidly reached their maximum output, whereas others produced a relatively linear output throughout overnight experiments. To maximize detection speed and sensitivity, we used the enzymatic reaction rate determined from the slope of absorbance at 570 nm over time to calculate fold change for the family of LacZ toehold switches (Figure 3C). As with the fluorescent reactions, paper-based reactions with colorimetric outputs can be arrayed for large-scale, quantitative experiments (Figure S3B).

Using switch D to demonstrate color development, detection of the reaction can be seen by the naked eye to begin at 25 min and saturates in ~1 hr (Figure 3D). Quantification of these reactions can also easily be done by measuring the intensity of the color channels red, green, and blue from images produced by most cameras, including those widely available in cellphones. By tracking the generation of signal in the blue channel, relative to yellow signal (red + green channels), the progress of the activated freeze-dried toehold switch reaction can be assessed and quantified (Figure 3E). Similar results were observed for the whole family of toehold switches (Figure 3B).

We have also incorporated an alternative colorimetric reporter enzyme, chitinase, into synthetic gene networks for systems based on extracts from cells that contain a LacZ background (Figure S3C). As demonstrated with our tetO-*GFP* and tetO-*mCherry* switches, the presence of aTc inducer results in the expression of chitinase, which cleaves a colorless substrate (4-Nitrophenyl N,N'-diacetyl-β-D-chitobioside) to yield a yellow p-nitrophenol product. The colorimetric output is visible to the naked eye and can be quantified using a standard plate reader

Figure 1. Paper-Based Synthetic Gene Networks

(A) The enzymes of transcription and translation are combined with engineered gene circuits and then embedded and freeze dried onto paper to create stable and portable synthetic gene networks outside of the cell. These networks are genetically encoded tools with trigger, regulatory transducer, and output elements.

(B) GFP expression in solution phase from fresh and freeze-dried PT7 cell-free reactions.

(C) Freeze-dried pellets of the PT7 cell-free expression system are stable for over a year at room temperature, yielding GFP expression in solution phase when rehydrated.

(D) A schematic of the constitutive *GFP* expression constructs used on paper.

(E) Images of paper discs following a 2 hr incubation and maximum fold-change measurements of constitutive paper-based GFP expression from freeze-dried S30, S30 T7, and PT7 cell-free systems during the first 90 min of incubation.

(F) Schematic of tetO regulation for *GFP* and *mCherry*.

(G) Images of paper discs following a 2 hr incubation and maximum fold-change measurements of GFP and mCherry from the tetO-regulated promoter during the first 2 hr of incubation ± aTc inducer (11 μM) from freeze-dried S30 reactions. BF indicates bright-field images, and F indicates fluorescence images.

Error bars represent SD.

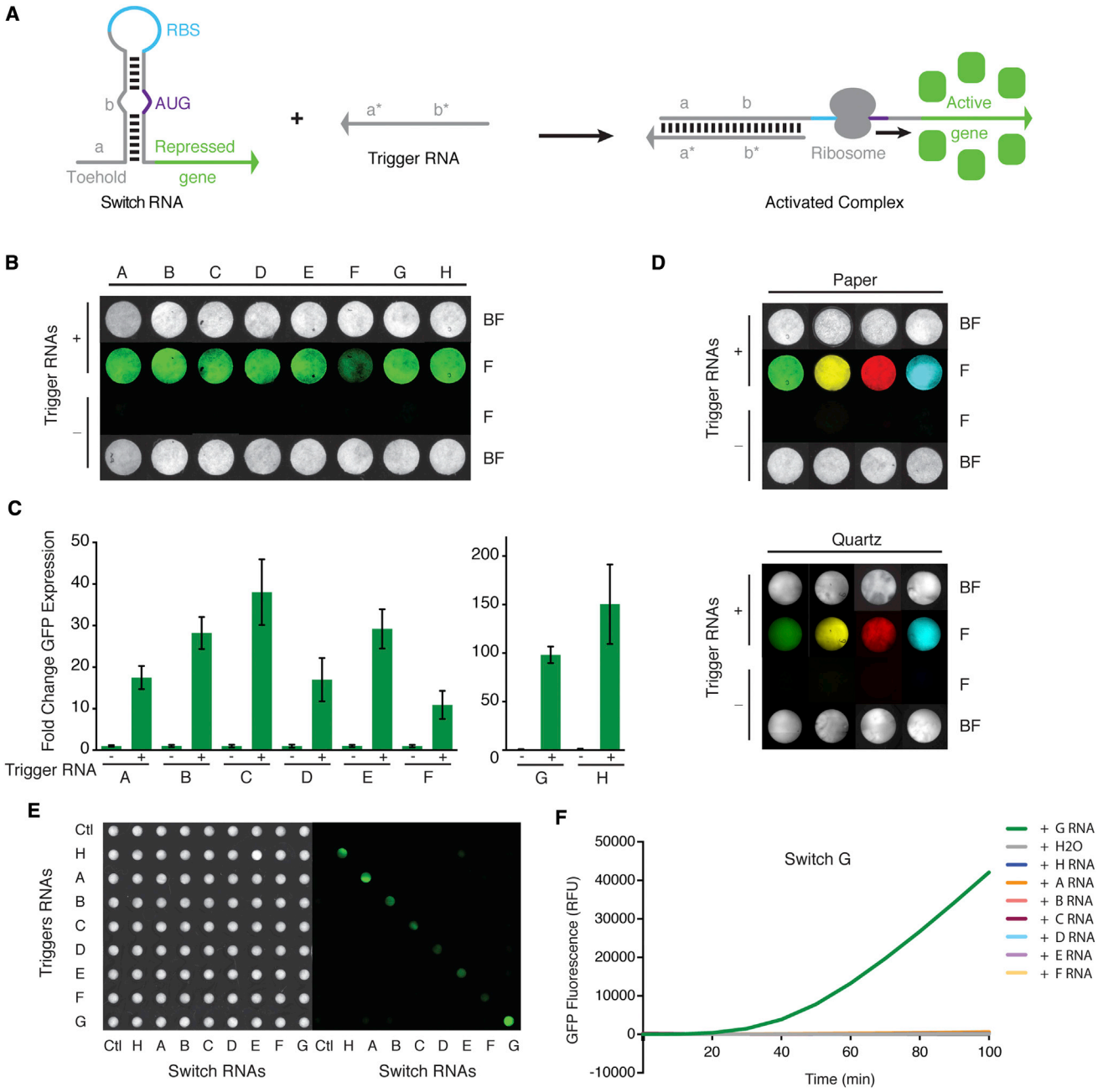

Figure 2. Freeze-Dried RNA-Actuated Gene Circuits on Paper

(A) Schematic of the RNA-based toehold switch regulating translation of GFP.

(B) Images of paper-based GFP expression from eight toehold switches (A–H) in the PT7 cell-free system, ± complementary trigger RNAs following a 2 hr incubation.

(C) Maximum fold-change measurement of GFP expression from paper-based toehold switches A-H during the first 90 min of incubation.

(D) RNA-actuated expression of GFP, Venus, mCherry, and Cerulean fluorescent proteins from toehold switch H on paper and quartz microfiber discs following a 2 hr incubation.

(E) Bright field and fluorescence images of an orthogonality screen between toehold switches and trigger RNAs using paper-based reactions arrayed in a 384-well plate. Images collected after the overnight data collection.

(F) Quantification of fluorescence over time from paper discs containing switch G (bottom row of the array). All data were generated from freeze-dried, cell-free reactions embedded into paper with their respective gene circuits. Trigger RNA concentration used for toehold switch activation was 5 μM. BF indicates bright-field images, and F indicates fluorescence images.

Error bars represent SD.

(410 nm; Figures S3D–S3F). Color development with this system was linear from the onset of detectable output at about 60 min, until the end of the experiment at 800 min, with a maximum induction of 38-fold at 420 min.

An important advantage of paper-based distribution of synthetic gene networks is their potential for low cost and relative ease to manufacture. As a proof-of-principle demonstration, we created printed arrays of stable synthetic gene networks using a standard computer printer and chromatography paper (Figure 3F). A commercially available wax-based ink serves as a hydrophobic barrier separating respective reaction spaces to create custom arrays and layouts (Carrilho et al., 2009). As a demonstration of the technique, we printed 5 × 5 arrays to host the freeze-dried LacZ-expressing toehold switch E and then rehydrated the array with and without trigger RNA to create a checkerboard pattern (Figure 3G).

For other practical applications, we built a low-cost electronic optical reader to enable quantification and ultimately automation of the paper-based reactions. Such a device could also impart these molecular devices with the ease of use and convenience of a home glucose monitor. To measure light transmission through these reactions, we placed LacZ-based toehold switches on paper discs between LED light sources (570 nm) and electronic sensors (Figure 3H). In the event of a positive reaction, light transmission is progressively blocked by the production of the purple LacZ cleavage product. LEDs and sensors were coordinated through multiplexers connected to an Arduino that controlled the read pattern and rate parameters (Figure S3G). Electronic hardware was housed using computer-designed parts laser cut from acrylic to create a device for under $100 USD (Figures 3H and S3H). Freeze-dried paper discs were placed into holes on a chip, rehydrated, incubated in the device at 37°C, and monitored in real time through an attached laptop. As a proof of concept, we tested the LacZ toehold switch G and observed consistent and significant reads from different concentrations of RNA trigger (Figure 3I).

An In Vitro Diagnostics Platform

With a device in hand, we next turned our focus to developing toehold switch sensors capable of detecting full-length active mRNA targets, a key feature for a diagnostics platform. Our first goal was the detection of GFP and mCherry mRNAs. Using an algorithm that predicts RNA secondary structure, mRNA sensors were built to target sequences likely to be accessible for binding (Green et al., 2014) and, when tested, yielded fluorescent induction in the presence of GFP (60-fold) and mCherry (13-fold) mRNAs, respectively (Figures 4B and 4C). As a demonstration of the potential for paper-based synthetic gene networks as an in vitro diagnostics platform, we next developed colorimetric mRNA sensors for antibiotic resistance genes (Figure 4A). In freeze-dried, paper-based reactions, mRNA sensors for spectinomycin (5-fold), chloramphenicol (7.5-fold), kanamycin (24-fold), and ampicillin (30-fold) resistance genes yielded significant LacZ induction in the presence of their respective mRNAs at 3,000 nM (Figures 4D and S4A). mRNAs used in these proof-of-concept experiments were provided in their purified form. However, given the fidelity of the toehold switches in the RNA-rich environment of the cell (Figure S2C; Green et al., 2014), we are confident that in vitro paper-based toehold sensors will exhibit similar specificity in the presence of mixed RNA samples.

Switching from the plate reader, we then tested the ampicillin resistance mRNA sensor using the electronic optical reader and found significant detection of target transcripts as low as 3 nM (Figures 4E and S4B). Moreover, the signal from our in-house device was about three times greater than the plate reader at equivalent trigger RNA concentrations (Figures 4D, 4E, and S4A).

In addition to the purpose-built synthetic gene networks presented above, this in vitro paper-based approach also holds tremendous potential for hosting other gene circuits, including those already in the literature as synthetic biology tools. Moreover, although the work above focused on bacterial components, the platform should in principle be readily extendible to mammalian-based systems. As confirmation, we tested a paper-based system using freeze-dried HeLa cell extracts and found strong expression of GFP in the presence of a constitutive expression plasmid (Figure 4F). To demonstrate the use of a pre-existing molecular tool, we chose to build a portable, in vitro glucose sensor on paper using a FRET-based nanosensor originally designed for measuring glucose in mammalian cells (Figure 4G; Takanaga and Frommer, 2010). The DNA construct for the nanosensor was freeze dried, along with HeLa cell extracts onto paper discs, and then rehydrated in the presence or absence of glucose. Upon rehydration, we observed the glucose-related shift previously reported in mammalian cells in our portable paper-based system within a physiologically relevant glucose concentration range (Figures 4H and S4C). Highlighting the stability of this FRET-based sensor, the SD of reads remains low even when compiled from data collected over a 100 min period. Importantly, de novo translation of the nanosensor seems to be critical to function because freeze-dried preparations of pretranslated protein did not exhibit the characteristic shift in fluorescence.

Rapid Sensor Prototyping

The low cost of manufacturing (4-65¢/sensor) is a key feature of the paper-based platform for diagnostics. However, perhaps even more important for the adoption and potential impact of this technology is the time and cost of developing new sensors. To test how rapidly new sensors could be developed, we chose to build mRNA sensors for the viral pathogen Ebola. Our goal was to construct and test 24 sensors that could distinguish between the Sudan and Zaire strains of the virus in under a day. Using our algorithm, sensors were designed to target mRNA from 12 regions (A–L) of the mRNA encoding the Ebola nucleoprotein, which differs in length by only three nucleotides between the Sudan and Zaire strains (Figure 5A). Construction began with PCR amplification of synthetic 135-nt DNA oligos bearing the toehold switch sensor cassettes, followed by ligation of the modules to our LacZ reporter chassis. The ligated product was then amplified by PCR. Followed by only column purification, sensors were tested on paper discs containing the freeze-dried PT7 cell-free system for testing in the presence and absence of 36 nt trigger RNAs. Here, we chose to add the sensor element during the rehydration phase of the experiment to demonstrate the potential for rapid prototyping and to highlight that the user does not need to know what sensors will be tested

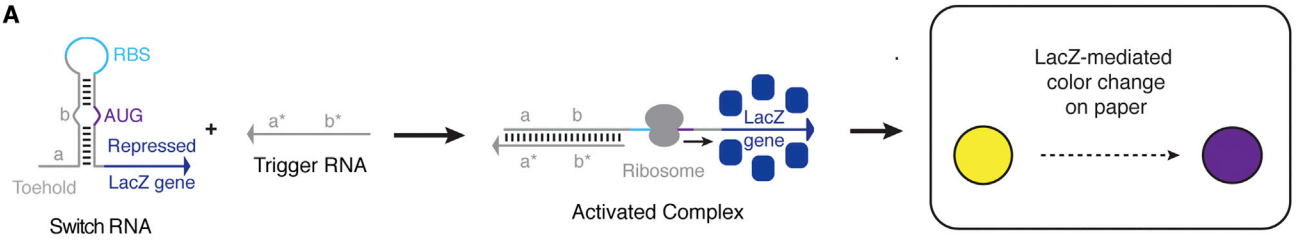

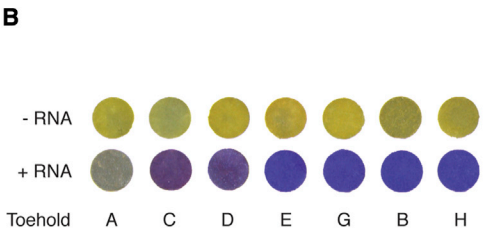

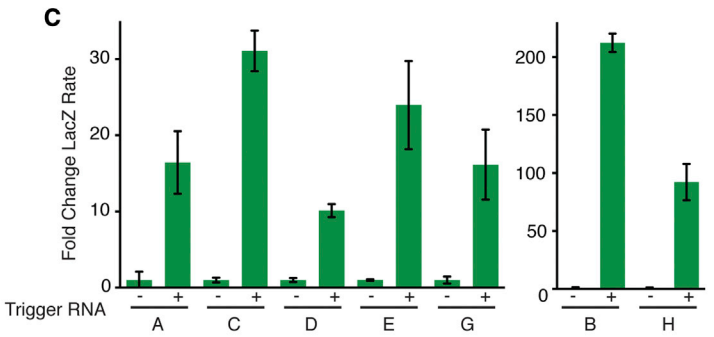

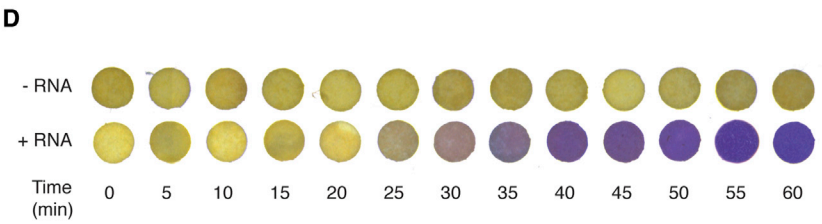

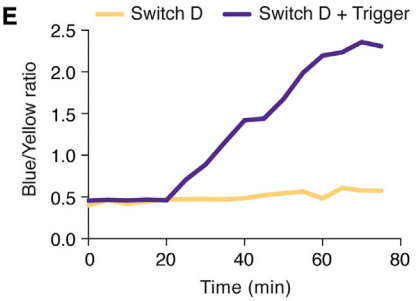

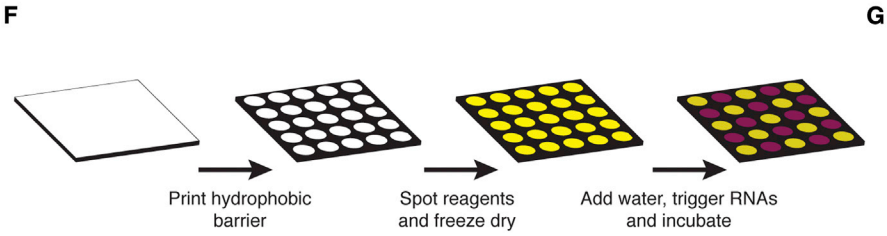

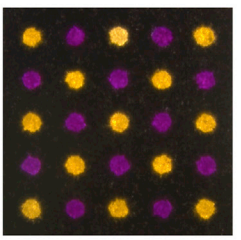

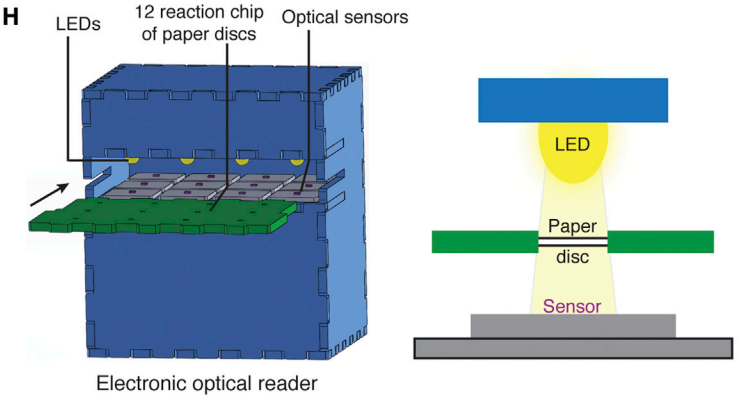

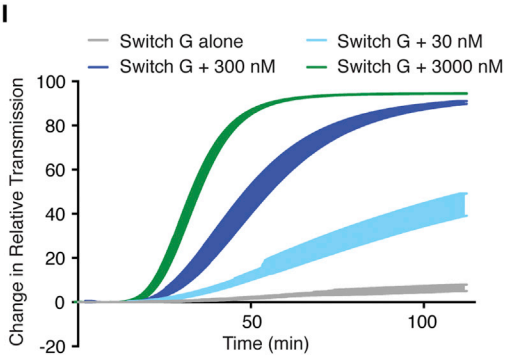

(legend on next page)

ahead of time, as might be the case with an emerging pathogen. Due to potential challenges with access to full-length material, we chose to use short 36 bp trigger RNAs rather than full-length mRNA to test the sensors. Although accessibility due to RNA secondary structure is important to keep in mind, work from our previous mRNA sensors suggests that short RNA triggers provide a representative indication of sensor function.

The colorimetric dynamics of the 240 reactions were captured using a plate reader and could be tracked by eye (Figures 5B and 5C). Each of the 24 sensors was triggered in the presence of their target (3,000 nM), with maximum induction during the first 90 min ranging 4- to 77-fold. Remarkably, beginning with the arrival of the DNA oligos, this phase of the screen was completed in less than 12 hr. We then selected four matching sets (D, E, G, and H) of the Sudan and Zaire sensors to test specificity and found a high degree of strain-specific discrimination (Figure 5D), as well as sensitivity down to a concentration of 30 nM trigger RNA for both strains (Figure 5E).

Rapid Prototyping and Testing of Complex Synthetic Gene Networks

As a demonstration of the capacity of the paper-based system for the prototyping and testing of more complex synthetic gene circuits, we assembled a converging transcription cascade that can convert the transcription activity of the native *E. coli* RNAP in a S30 cell extract into T3 and/or T7 RNAP activity (Figure 6A). To this point, we have validated the paper-based system using more than 45 toehold switches, each with unique combinations of inputs and measureable outputs. Here, we assembled toehold switches to create a series of molecular reactions that lead to the de novo production of transcriptional tools. In the presence of DNA encoding the toehold switch and trigger for the T3 module, T3 RNAP is transcribed and translated, which activates T3-mediated transcription and translation of GFP from an otherwise passive component (Figure 6B). Alternatively, in the presence of DNA encoding the toehold switch and trigger for the T7 module, T7 RNAP is transcribed and translated, leading to the expression of GFP from a T7-dependent promoter (Figure 6C). If both the T3 and T7 toehold switch modules are combined, *E. coli* RNAP generates both T3 and T7 RNAPs. This converging transcription activity leads to their respective trigger and toehold switch RNAs, producing a third route to GFP expression (Figure 6D). This work shows that the platform can sustain multiple rounds of transcription and translation and be utilized to construct, test, and debug complex circuits in a modular fashion.

DISCUSSION

We have developed a method for embedding synthetic gene networks into paper and other porous materials, creating a much-needed path for moving synthetic biology out of the lab and into the field. Here, we have constructed a number of purpose-built synthetic gene networks responsive to synthetic RNA, mRNA, and small molecules. This includes paper-based toehold switches, which generate networks with greater than 20-fold (Figures 2C and 3C) and as high as 350-fold induction (Figure S2F). As demonstrated with the glucose sensor, this paper-based approach also promises to convert existing constructs designed for basic research and biotechnology into portable and readily accessible molecular tools (Figures 4G and 4H).

The in vitro nature of these reactions affords many benefits. For instance, without having to contend with maintaining the plasmid over generations of cell division, complex genetically encoded networks can be assembled without the need for coordinating selective antibiotic pressures. Moreover, paper-based reactions can serve as a mock cell, allowing for linear PCR products to be screened directly for function without sequencing, assembly into circularized plasmids, or even gel purification of fragments. We took advantage of these features in our paper disc arrays to measure toehold orthogonality, as well as Ebola sensor prototyping and complex circuit testing (Figures 2E and 2F, 5, 6, S2G, S2H, and S3B), which allowed us to rapidly screen for gene circuit performance.

The paper-based cell extracts also offer a unique opportunity for molecular biologists to work with difficult-to-culture organisms. By generating cell extracts from engineered cell lines, pathogens, or other specialized organisms (e.g., extremophiles and symbionts), these reactions could serve as a proxy for biology that is otherwise inaccessible to the broad research community. Similarly, the incorporation of human cell extracts into our paper-based scheme is an exciting feature that leads to the prospect of diagnostic and synthetic biology applications based on the thousands of human and mammalian transcription

Figure 3. Colorimetric Output from Paper-Based Synthetic Gene Networks

(A) A schematic of the modified, LacZ-expressing toehold switches used to generate colorimetric outputs.

(B) Images of the paper-based, colorimetric output from toehold switches ± complementary RNA triggers following a 2 hr incubation.

(C) Maximum fold-change measurements from LacZ toehold switches during the first 2 hr of incubation. Fold induction based on the rate of color change from LacZ toehold switches.

(D) The paper-based development of color from LacZ toehold switch D over 60 min.

(E) Color intensities from (D) were converted to a ratio of blue over yellow (red + green channels) channels and graphed over time.

(F) Schematic describing the process of arraying synthetic gene networks on paper using printed arrays.

(G) A 25-reaction printed array (14 × 14 mm) of toehold switch E, containing positive reactions (purple) and negative control reactions (yellow) distributed in a checkerboard pattern following a 2 hr incubation.

(H) Schematic of the low-cost, electronic optical reader developed to read colorimetric output from paper-based synthetic gene networks. Paper reactions held in a chip between an LED light source (570 nm) and electronic sensor.

(I) Time-course data from the electronic optical reader of toehold switch G in the presence of 0, 30, 300 and 3,000 nM trigger RNA. Data were collected every 10 s with SD indicated by line thickness, and all data were generated from freeze-dried, cell-free reactions embedded into paper with their respective gene circuits. Trigger RNA concentrations used for toehold switch activation were 5 μM or as specified.

Error bars represent SD.

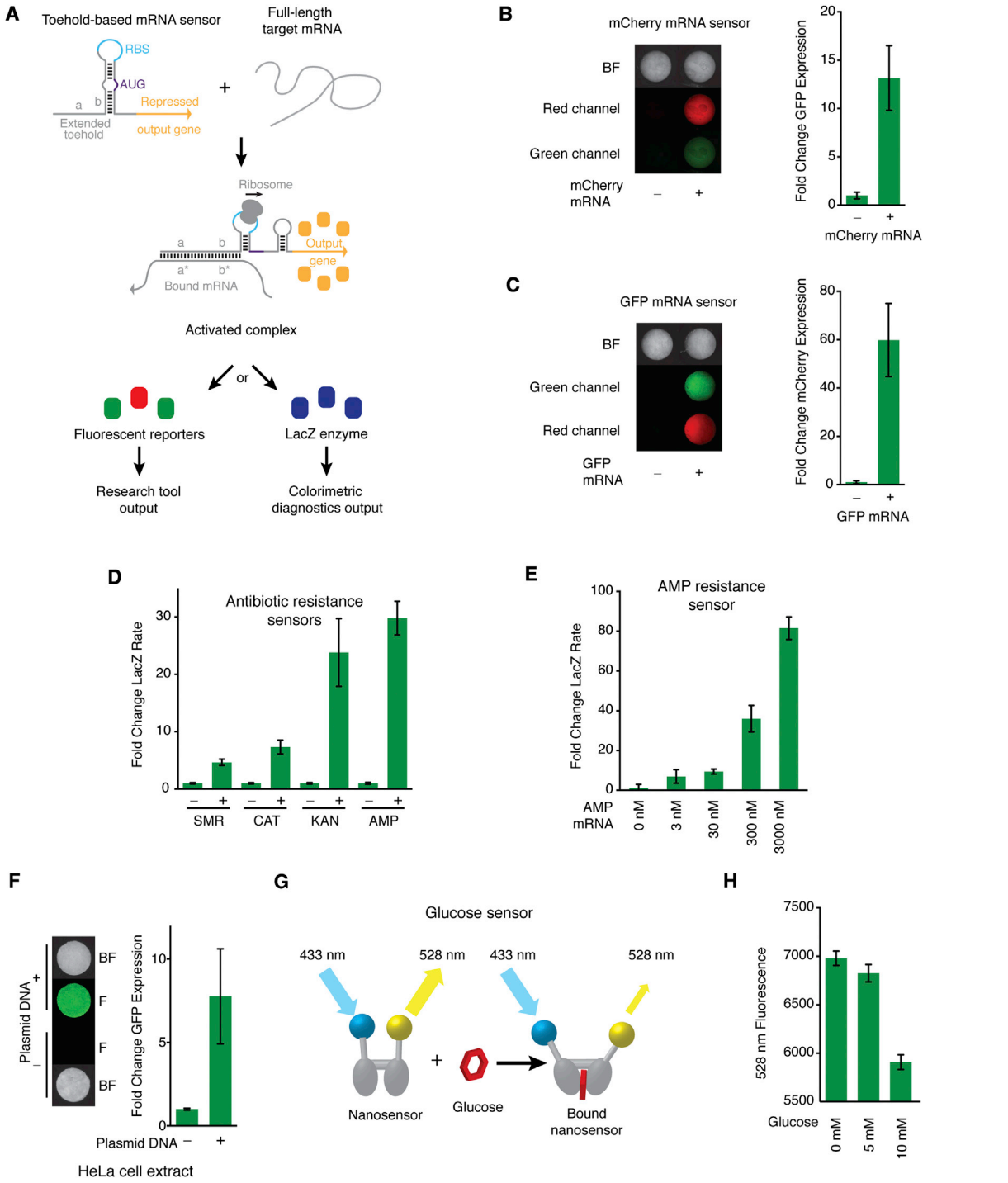

Figure 4. Application of Paper-Based Synthetic Gene Networks

(A) Schematic of the paper-based mRNA sensors based on toehold switches.

(B) Images and fold-change measurements of a paper-based mCherry mRNA sensor in the presence and absence of full-length target mRNA, following a 2 hr incubation. GFP is produced in response to detection of mCherry mRNA.

(C) Images and fold-change measurements of a paper-based GFP mRNA sensor in the presence and absence of full-length target mRNA. mCherry is produced in response to detection of GFP mRNA.

(D) Maximum fold change during the first 90 min of the LacZ-mediated color output rate from sensors for mRNAs encoding resistance to spectinomycin, chloramphenicol, ampicillin, and kanamycin antibiotics using a plate reader.

(legend continued on next page)

factors (Hughes, 2011), such as nuclear receptors, with complex and nuanced regulatory features, including small-molecule-responsive regulation (Pardee et al., 2011).

Perhaps most exciting is the potential to bring the rational design approach of synthetic biology to in vitro diagnostics and sensing. Although competing antibody-based technologies such as rapid diagnostic tests (RDTs) currently have greater sensitivity, we expect advances in molecular techniques and analyte concentration methods to solve these challenges. Examples of existing technologies that could be implemented as part of the platform include isothermal nucleic acid sequence-based amplification of target RNA inputs (Yan et al., 2014) or concentration of pathogen through generic opsonin-mediated capture (Cooper et al., 2014; Kang et al., 2014). Moreover, rather than competing with technically demanding and expensive lab-based techniques like ELISA, PCR, and mass spectrometry, we envision paper-based systems creating a new, low-cost generation of sensors that could be embedded ubiquitously into daily life (including clothing). Importantly, we were able to run toehold switch reactions in a variety of porous materials, including cloth, lab membranes, and porous alumina (data not shown).

Unlike antibody-based diagnostics, toehold switch mRNA sensors offer a sequence-based method of detection that means research and clinical tools can be designed rationally, lowering development costs and allowing for significantly shorter design-to-production cycles. Here, we presented toehold-based mRNA sensors, including 24 Ebola sensors that were constructed in less than 12 hr. The DNA input cost for the Ebola series was $21 USD/sensor. These features compare highly favorably to custom commercial antibody production, where development time is typically 2 to 6 months and development costs range from $4,000 to $30,000 USD. Further, sensors can be designed from sequence information alone, which is ideal for emerging pathogens (Figure 5), and the acquisition of other relevant clinical information, such as the presence of drug-resistance genes (Figures 4D and 4E) or other indicators of pathogenesis, such as biofilm-specific RNAs (Dötsch et al., 2012). Coupled to an electronic reader, these paper-based systems also offer the potential for quantitative diagnostics (Figures 3I and 4E), a much-needed feature that is largely unavailable with RDTs (Cordray and Richards-Kortum, 2012). Moreover, the added sensitivity (2.5–3.5 ×) of our purpose-built, electronic reader could be considered a hardware enhancement of the designed gene circuits (Figures 4E and S4A).

Paper-based synthetic gene networks are also potentially less expensive to manufacture than most of the standard of care options currently available. At the moment, the cost of a 1μl paper-based sensor would be between 35¢ and 65¢ using commercial cell-free expression systems. However, these systems can be readily produced in house, reducing the cost to as little as 2¢ to 4¢ per sensor (Noireaux, 2013). This compares to $0.45 to $1.40 for a single RDT reaction and $1.50 to $4.00 (reagents only) for PCR (Cordray and Richards-Kortum, 2012). Transcription- and translation-based detection is also competitive with regards to time to detection. As an example, detection of mRNA from the ampicillin resistance gene was recorded as early as 25 min for high concentrations of mRNA and about 40 min for our 3 nM treatment (Figures 4E and S4B). This compares favorably to RDTs, which can detect a single antigen in ~20 min or PCR, which can take at least 1 hr and is largely confined to laboratory settings (Cordray and Richards-Kortum, 2012).

Our construction and testing of a converging transcription cascade on freeze-dried paper discs (Figure 6) further underscores the potential of this approach to host complex network reactions for both laboratory and field applications. Although perhaps not at first obvious, for each of the three transcription cascade reactions to produce GFP (Figures 6B–6D), the system had to essentially cycle through two cycles of the central dogma. The first cycle converts the DNA of the cascade module(s) to RNA and then protein (RNAP), which sets off the second cycle that converts the DNA of dormant reporter to RNA and then protein (GFP). Thus, despite their small size, the paper discs have the transcription and translation capacity required for complex tasks. For synthetic biology applications, such a transcription cascade could be used to build more sophisticated networks with layers of outputs that remain inactive unless triggered by a circuit producing the correct RNAP. Further, as the orthogonality (Figures 2E, S2G, S2H, and S3B) and Ebola screens showed (Figure 5), the paper-based system has significant potential to increase the pace at which genetically encoded tools can be built and tested. With this in mind, we foresee this technology being extended to prototyping of engineered metabolic pathways and other complex gene circuits as a way to rapidly vet combinatorial designs before moving to cellular hosts. Thus, ready-to-use paper-based systems could not only make tools currently only available in the laboratory readily fieldable but also improve the development of new tools and the accessibility of these molecular tools to educational programs for the next generation of practitioners.

Taken together and considering the projected cost, reaction time, ease of use, and no requirement for laboratory infrastructure, we envision paper-based synthetic gene networks significantly expanding the role of synthetic biology in the clinic, global health, industry, research, and education.

(E) Maximum fold change during the first 90 min of the color output rate from the ampicillin resistance sensor using the in-house electronic optical reader over a titration of mRNA concentrations.

(F) Images of paper discs following a 2 hr incubation and fold-change measurement of constitutive paper-based GFP expression from a freeze-dried HeLa cell extract.

(G) Schematic of the FRET-based mechanism used in the glucose nanosensor.

(H) Using an average of the data collected every 10 min between 390 min and 490 min, the 528 nm fluorescence is reduced in response to glucose binding to the FRET-based glucose nanosensor expressed on paper. All data were generated from freeze-dried, cell-free reactions embedded into paper with their respective gene circuits.

Error bars represent SD.

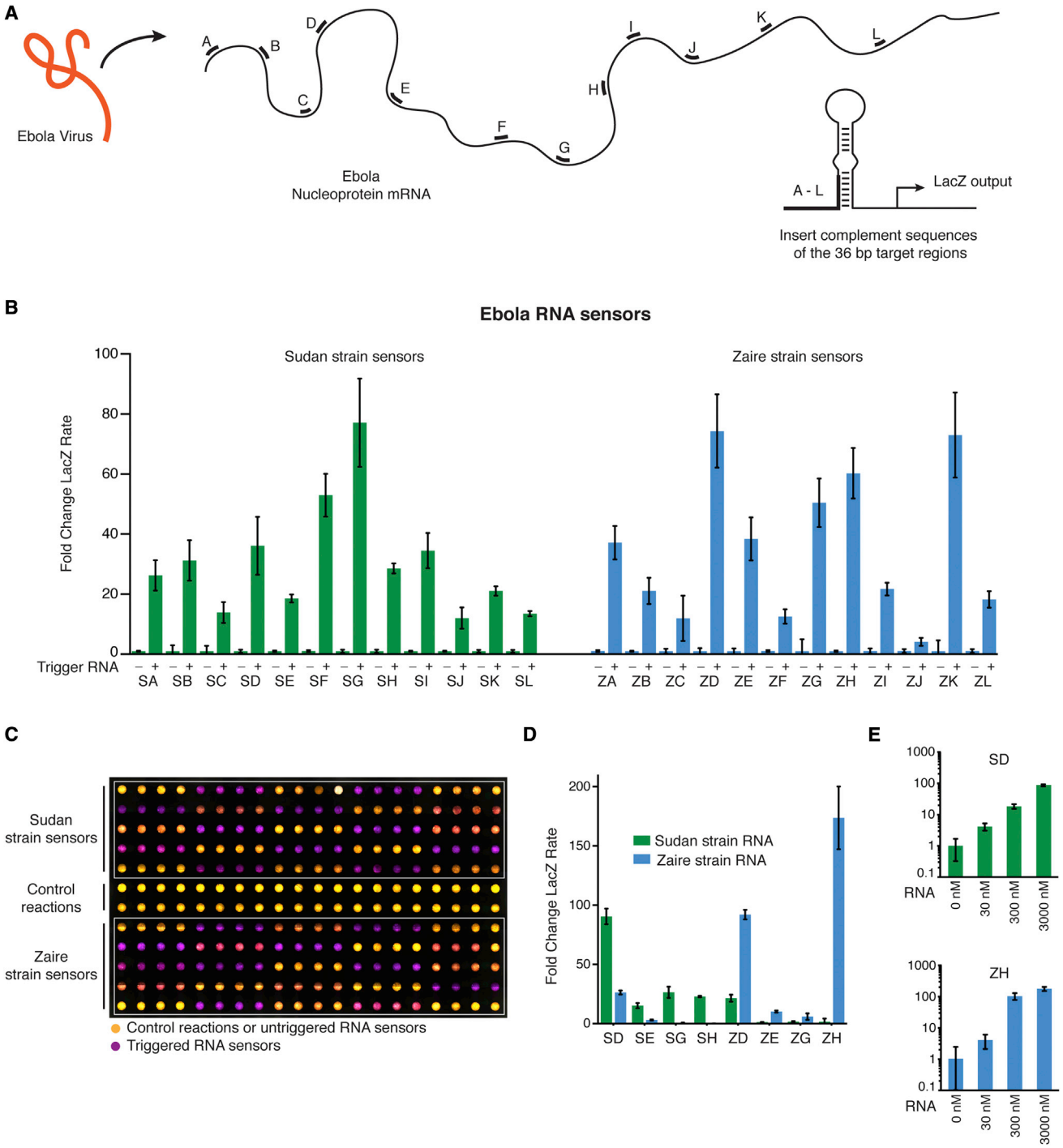

Figure 5. Rapid Prototyping of Paper-Based RNA Sensors for Sequences from Sudan and Zaire Strains of the Ebola Virus

(A) Schematic of the generation of Ebola RNA sensors. Sensors with the same letter were targeted to identical windows in the Ebola nucleoprotein mRNAs of their respective strains.

(B) Twenty-four toehold switch-based RNA sensors were constructed and tested in a 12 hr period. Based on the RNA segment windows (A–L), maximum fold change during the first 90 min at 37°C is reported for both the Sudan and Zaire strains of the virus. Fold change rate is determined from the slope of absorbance at 570 nm over time (– control, + 3000 nM RNA trigger).

(C) Composite image of the 240 paper-based reactions used to test the 24 sensors after data collection overnight. Control and untriggered toehold sensors remain yellow, and activated toehold sensors have turned purple.

(legend continued on next page)

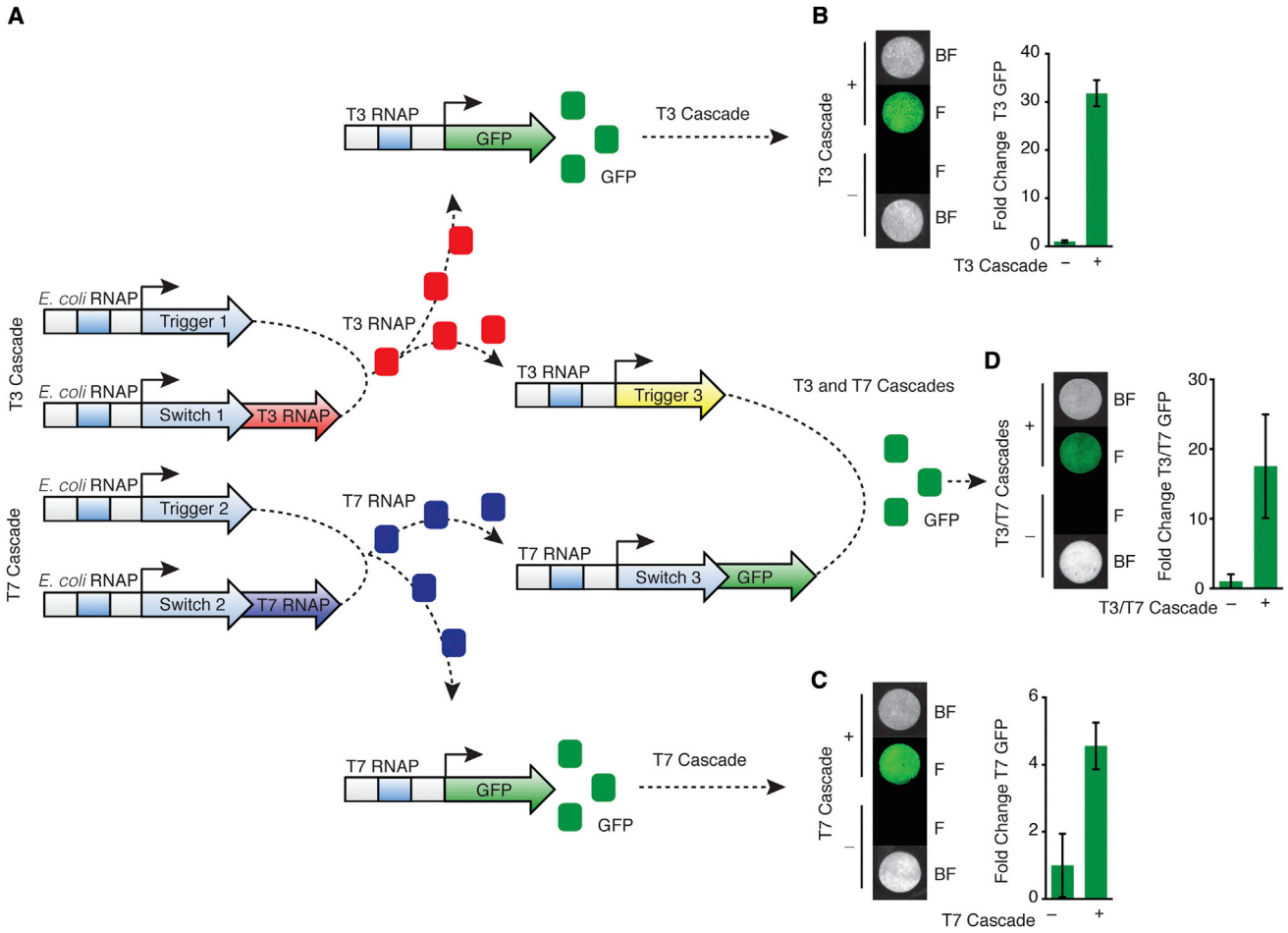

Figure 6. Paper-Based Converging Transcriptional Cascade

(A) Schematic of the genetically encoded components that convert transcription from *E. coli* RNAP into transcription from T3 RNAP and/or T7 RNAP. Expression of these new RNAPs drives the transcription of previously dormant *GFP* constructs containing T3 or T7 promoters, and alternatively, they can drive expression of a toehold switch and trigger pair under the regulation of T7 and T3, respectively.

(B) Images and fold-change measurements of paper-based T3 GFP expression with and without the T3 cascade module.

(C) Images and fold-change measurements of paper-based T7 GFP expression with and without the T7 cascade module.

(D) Images and fold-change measurements of paper-based T3/T7-dependent GFP expression with and without the T3 and T7 cascade modules. All data were generated from freeze-dried, cell-free reactions embedded into paper with their respective *GFP* expression constructs; cascade modules were added as DNA components at rehydration. Data were collected after an overnight incubation.

Error bars represent SD.

EXPERIMENTAL PROCEDURES

TetR-Based Inducible Synthetic Gene Circuits

The TetR-based GFP, mCherry, and chitinase expression circuits were constructed by inserting *GFP*, *mCherry*, or *chitinase* downstream of the TetR-repressed pLtetO promoter in pZE11 (Lutz and Bujard, 1997). To provide constitutive TetR expression, *TetR* was cloned downstream of the constitutive placIQ promoter, and this expression cassette was inserted into pZE11-gfp and pZE11-mcherry using XhoI and AatII.

Toehold Switch Construction

Toehold switch plasmids were constructed using conventional molecular biology techniques. Synthetic DNA templates (Integrated DNA Technologies) were amplified using PCR, inserted into plasmids using Gibson assembly (Gibson et al., 2009) with 30 bp overlap regions, and then successfully constructed plasmids identified using DNA sequencing. All plasmids were derived from pET system parent plasmids (EMD Millipore) and constitutively express *lacI* and antibiotic resistance genes. Additional descriptions of the toehold switch plasmids and their sequences are provided in Green et al. (2014).

(D) Sequence specificity tested for four Sudan and four Zaire sensors from the original set of 24. Each of the four sensors targeting Sudan sequences were treated with 3,000 nM of off-target RNA sequence from the complementing Zaire RNA sequence and vice versa.

(E) Fold change of the color output rate of sensors SD and ZH over a titration of RNA concentrations. All data were generated from freeze-dried, cell-free reactions embedded into paper. DNA containing the sensor and RNA triggers was added during rehydration.

Error bars represent SD.

Preparation of Matrix Materials

Although our initial paper-based reactions were successful, we suspected that nonspecific interactions between the components of the cell-free system and the cellulose matrix of paper could be impeding the activity of the reactions. Cellulose holds a pH-dependent charge (Budd, and Herrington, 1989), and thus it seemed likely that components from the complex biomolecular systems could adsorb to the high surface area of cellulose fibers, reducing reaction efficiency. Accordingly, we treated the filter paper with bovine serum albumin (BSA) and other commonly used blocking reagents. We found an overall improvement in fluorescent output from treated paper, with 5% BSA yielding the greatest increase (Figures S5A and S5B). For quartz microfiber, an alternate substrate, the performance enhancement of blocking with the surfactant Tween-20 was even more pronounced (Figures S5C and S5D).

Cell-Free Reactions

Cell-free reactions were assembled (4°C) as generally described in the instructions of the respective manufacturers and then immediately incubated at 37°C. Briefly, for S30 and S30T7 reactions (Promega, L1020 and L1110), cell extracts and premix containing amino acids were combined at a ratio of 0.33 and 0.51, respectively. The volume was then brought up with RNase inhibitor (Roche; 0.005), plasmid DNA constructs comprising the gene circuits, and nuclease-free ddH_2O. For tetO-based gene circuits, reactions were supplemented with prerun cell-free reactions expressing constitutive TetR (0.05) to reduce promoter leakage. For the PT7 cell-free system (NEB, E6800L), solutions A (0.4) and B (0.3) were combined together, with the remaining volume composed of RNase inhibitor (Roche; 0.005), linear DNA constructs, and nuclease-free ddH_2O. HeLa cell cell-free systems (Thermo Scientific, 88881) were assembled by combining HeLa cell lysate (0.5), accessory proteins (0.1), and reaction mix (0.2) with RNase inhibitor (Roche; 0.005), plasmid DNA constructs comprising the gene circuits, and nuclease-free ddH_2O. Long-term storage of freeze-dried pellets was done protected from light, under nitrogen gas and in the presence silica gel desiccation packages. For colorimetric reactions, the enzymatic substrates chlorophenol red-β-D-galactopyranoside and 4-Nitrophenyl N,N'-diacetyl-β-D-chitobioside were supplied to the reactions prior to freeze drying at final concentrations of 0.6 mg/ml and 3 mg/ml, respectively.

The concentration for the gene circuits were as follows: Figures 1B and 1C, T7_GFP plasmid DNA 5 ng/μl (pBR939b_T7_GFP; Anderson et al., 2007); Figure 1E, PN25-GFP plasmid DNA 30 ng/μl and T7_GFP plasmid DNA 30 ng/μl; Figure 1G, TetO-GFP and TetO-mCherry plasmid DNA 30 ng/μl. Toehold switch and sensor sequences are available as a supplemental information file (Data S2); Figure 2, linear DNA 33 nM, RNA triggers 5 μM; Figure 3, linear DNA 33 nM, RNA triggers 5 μM or as specified; Figures 4B and 4C, mCherry and GFP mRNA sensors linear DNA 33 nM, respective mRNAs 2.5 μM; Figures 4D and 4E, antibiotic resistance gene mRNA sensors for spectinomycin, chloramphenicol, kanamycin, and ampicillin linear DNA 33 nM, respective mRNAs 3 μM or as specified; Figure 4F, pT7CFE1_GFP plasmid DNA (Thermo Scientific) 30 ng/μl, pcDNA3.1 FLIPglu-30uDelta13V plasmid DNA (Takanaga and Frommer, 2010; Addgene:18015) 30 ng/μl; Figure 5, PCR product was not gel purified, so a 5× linear DNA concentration of 150 ng/μl was used to ensure adequate sensor product, respective trigger RNAs 3 μM or as specified; Figure 6, T3 and T7 cascade modules plasmid DNA 30 ng/μl (*E. coli* RNAP_trigger_1, *E. coli* RNAP_switch_1_T3RNAP, *E. coli* RNAP_trigger_2, *E. coli* RNAP_switch_2_T7RNAP), T3_GFP and T7_GFP plasmid DNA 40 ng/μl, T3 RNAP_trigger_3, and T7 RNAP_switch 3_GFP plasmid DNA 40 ng/μl.

Preparation of Reactions and Incubation

Assembled cell-free reactions were applied (1.8 μl/disc) to 2 mm paper discs (Whatman, 1442-042), which were then flash frozen in liquid nitrogen and freeze dried overnight. Paper discs were cut using a 2 mm biopsy punch. Similarly, quartz microfiber (Spectrum, 884-66171) was cut and treated with cell-free reactions (3 μl/disc) prior to freeze drying. Freeze-dried solution phase reactions (7 μl) were similarly flash frozen and placed on the lyophilizer to create pellets. After 24 hr, paper reactions for Figures 1, 2, 3, and 4 were rehydrated with either nuclease-free ddH_2O or inducer at the concentrations specified. For these reactions, DNA for gene circuits was added to paper before freeze drying. For Figure 5 reactions, DNA containing the sensor and RNA triggers were both added during rehydration. For Figure 6 reactions, DNA for the GFP reporters were added prior to freeze drying (T3_GFP, T7_GFP, or T3/T7_GFP). Rehydration of the paper discs was then done in the presence or absence of DNA constructs for the T3 and/or T7 cascade modules. Cell-free reactions without synthetic gene networks were also included to provide the background signal for subtraction from control and treatment reactions. Rehydrated reactions were incubated at 37°C using either a plate reader (BioTek NEO HTS) or our in-house electronic optical reader placed inside a tissue culture incubator. For the plate reader, paper discs were placed into black, clear-bottom 384 well plates, and for the in-house reader, paper discs were placed into 2 mm holes in the removable acrylic chip (Figures 3H and S3H). Cell-based reactions presented in Figure S2C were performed in *E. coli* as described by Green et al. (2014). Briefly, log-phase cultures containing a toehold switch construct and either an on-target or off-target IPTG-inducible RNA trigger construct were diluted 1:100. Cells were grown at 37°C overnight in the presence or absence of 1 mM IPTG, and GFP expression was measured using a plate reader.

Microscopy and Image Processing

Images of paper discs were collected on a Zeiss Axio Zoom V16 Macroscope (magnification 7×) with an AxioCam MRm in a humidified glass chamber or through the bottom of a clear-bottom 384-well plate. Collected images were then stitched together using Zeiss Zen software into large composite images for further processing in ImageJ. Experiments were arranged so that images of matching control and treatment paper-based reactions were collected together such that parameters could be adjusted for all samples simultaneously. Once optimized, images of individual paper discs were cropped and arrayed into figures. For GFP expression in the S30 cell-free system, which exhibits a high level of autofluorescence, we used a Nuance camera to collect multispectral images between 500 and 620 nm. Perkin Elmer Nuance 3.0.2 software was then used to unmix the spectral signature of the GFP from that of the cell extract. A similar approach was used to create a absorbance signature (420 to 720 nm) for imaged paper discs with p-nitrophenol, the chitinase cleavage product of 4-Nitrophenyl N,N'-diacetyl-β-D-chitobioside. Images collected with the Nuance camera were scaled using bilinear transformation. For a few composite images, areas around the paper discs were masked to remove extraneous signal.

Printed Arrays

Patterns for printed arrays were generated using Adobe illustrator and then printed onto chromatography paper (Whatman, 3001-861) using a Xerox 8570 printer (Carrilho et al., 2009). Once printed, the wax was reflowed using a hot plate (120°C) so that the wax was present throughout the entire thickness of the paper, creating hydrophobic barriers to contain each reaction. The printing was performed at the Center for Nanoscale Systems at Harvard University, a member of the National Nanotechnology Infrastructure Network (NNIN), which is supported by the National Science Foundation under NSF award ECS- 0335765.

Electronic Optical Reader

The portable device consists of four layers housed within a laser-cut acrylic box (Figure 3H). The top layer holds 12 LEDs (Digi-Key, 754-1262-ND), which have a very narrow viewing angle and an emission of 570 nm to match the absorbance maximum of the product of the LacZ reaction. The LEDs were placed in close proximity to the chip in the middle layer, which holds 12 paper disks within 2 mm apertures. The apertures prevented transmission of stray light and were coaxial with the LEDs in the top layer and the array of 12 TSL2561 sensors (Adafruit, 439) in the third layer below. The bottom layer contains the Arduino Micro and associated electronics such as the multiplexers (Sparkfun, BOB-09056), breadboard, resistors, and connectors. To prevent crosstalk between reads, reactions were read in series by sequentially activating each LED and sensor pair. The read frequency and pattern of the reader can be easily adjusted by modifying and uploading alternative sketches to the Arduino Micro. Both the raw data and the data processed using the per disc formula: 100-(100*(Current/Max)) were calculated for each time point and sent to a laptop. A diagram of the circuit and an overview of the laser cut parts can be found in the supplemental figures (Figures S3G and S3H) and laser

cutting patterns and Arduino sketch files are provided as supplemental information files (Data S1).

Calculation of Fold Change

Fluorescence and absorbance data were first smoothed to reduce measurement noise using a moving three-point average of the time point and the data both preceding and following that read. Background signal was subtracted from each well using the average of control blank reactions that contained the relevant cell-free system alone. The minimum value of each well was then adjusted to zero. For fluorescence data, fold change calculations were done by dividing the wells at each time point by the average signal from the corresponding uninduced control wells. For absorbance measurements, fold change values reflect the difference in the rate of color change between induced and uninduced wells. This was done by calculating the rate of change using slope; therefore, at each 10 min time point, the rate reported was calculated as follows: $S_n = (T_{n+1} - T_n)/10$, where T is the normalized data at a time point (T_n) and the time point 10 min later (T_{n+1}), and S_n is the slope reported for T_n. Fold change was then calculated as with the fluorescence data. Experiments were run in either triplicate or quadruplicate. Due to high autofluorescence of the S30 reactions, a few experiments exhibited high variability and were accordingly subjected to the Modified Thompson Tau Test to identify outliers to be discarded (Anbarasi et al., 2011; Byrd et al., 2014). Briefly, the Tau test was performed by calculating the difference (delta) between a measured value (replicate) and the mean of the group. Using the Modified Thompson Tau value for quadruplicate data (1.4250), the test was performed by multiplying the SD of the group by this Tau value. If the resulting number was smaller than the delta calculated for a measured value, that replicate was considered an outlier and was not included in the analysis.

SUPPLEMENTAL INFORMATION

Supplemental Information includes Extended Experimental Procedures, five figures, and two data files and can be found with this article online at http://dx.doi.org/10.1016/j.cell.2014.10.004.

ACKNOWLEDGMENTS

K.P. is a Canadian Institutes of Health Research-funded postdoctoral fellow at the Wyss Institute at Harvard University. This work was supported by the Wyss Institute; and NIH Director's New Innovator Award (1DP2OD007292), an ONR Young Investigator Program Award (N000141110914), and an NSF Expedition in Computing Award (CCF1317291) through P.Y. and the Howard Hughes Medical Institute, the Office of Naval Research MURI program, and the Defense Threat Reduction Agency grant HDTRA1-14-1-0006 through J.J.C.

Received: September 10, 2014
Revised: September 29, 2014
Accepted: October 3, 2014
Published: October 23, 2014

REFERENCES

Anbarasi, M.S., Ghaayathri, S., Kamaleswari, R., and Abirami, I. (2011). Outlier Detection for Multidimensional Medical Data. Int. J. Comp. Sci. Info. Tech. *2*, 512–516.

Anderson, J.C., Voigt, C.A., and Arkin, A.P. (2007). Environmental signal integration by a modular AND gate. Mol. Syst. Biol. *3*, 133.

Budd, J., and Herrington, T.M. (1989). Surface charge and surface area of cellulose fibres. Colloids Surf. *36*, 273–288.

Byrd, K.B., O'Connell, J.L., Tommaso, S.D., and Kelly, M. (2014). Evaluation of sensor types and environmental controls on mapping biomass of coastal marsh emergent vegetation. Remote Sens. Environ. *149*, 166–180.

Callura, J.M., Dwyer, D.J., Isaacs, F.J., Cantor, C.R., and Collins, J.J. (2010). Tracking, tuning, and terminating microbial physiology using synthetic riboregulators. Proc. Natl. Acad. Sci. USA *107*, 15898–15903.

Callura, J.M., Cantor, C.R., and Collins, J.J. (2012). Genetic switchboard for synthetic biology applications. Proc. Natl. Acad. Sci. USA *109*, 5850–5855.

Carrilho, E., Martinez, A.W., and Whitesides, G.M. (2009). Understanding wax printing: a simple micropatterning process for paper-based microfluidics. Anal. Chem. *81*, 7091–7095.

Cooper, R.M., Leslie, D.C., Domansky, K., Jain, A., Yung, C., Cho, M., Workman, S., Super, M., and Ingber, D.E. (2014). A microdevice for rapid optical detection of magnetically captured rare blood pathogens. Lab Chip *14*, 182–188.

Cordray, M.S., and Richards-Kortum, R.R. (2012). Emerging nucleic acid-based tests for point-of-care detection of malaria. Am. J. Trop. Med. Hyg. *87*, 223–230.

Dötsch, A., Eckweiler, D., Schniederjans, M., Zimmermann, A., Jensen, V., Scharfe, M., Geffers, R., and Häussler, S. (2012). The Pseudomonas aeruginosa transcriptome in planktonic cultures and static biofilms using RNA sequencing. PLoS ONE *7*, e31092.

Elowitz, M.B., and Leibler, S. (2000). A synthetic oscillatory network of transcriptional regulators. Nature *403*, 335–338.

Fossati, E., Ekins, A., Narcross, L., Zhu, Y., Falgueyret, J.P., Beaudoin, G.A., Facchini, P.J., and Martin, V.J. (2014). Reconstitution of a 10-gene pathway for synthesis of the plant alkaloid dihydrosanguinarine in Saccharomyces cerevisiae. Nat Commun. *5*, 3283.

Gardner, T.S., Cantor, C.R., and Collins, J.J. (2000). Construction of a genetic toggle switch in Escherichia coli. Nature *403*, 339–342.

Gibson, D.G., Young, L., Chuang, R.-Y., Venter, J.C., Hutchison, C.A., 3rd, and Smith, H.O. (2009). Enzymatic assembly of DNA molecules up to several hundred kilobases. Nat. Methods *6*, 343–345.

Green, A.A., Silver, P.A., Collins, J.J., and Yin, P. (2014). Toehold switches: de-novo-designed regulators of gene expression. Cell *159*, this issue, 925–939.

Hong, S.H., Ntai, I., Haimovich, A.D., Kelleher, N.L., Isaacs, F.J., and Jewett, M.C. (2014). Cell-free protein synthesis from a release factor 1 deficient Escherichia coli activates efficient and multiple site-specific nonstandard amino acid incorporation. ACS Synth. Biol. *3*, 398–409.

Hughes, T., ed. (2011). Handbook of transcription factors. Subcellular Biochemistry, First Edition, *Volume 52* (New York: Springer).

Isaacs, F.J., Dwyer, D.J., Ding, C.M., Pervouchine, D.D., Cantor, C.R., and Collins, J.J. (2004). Engineered riboregulators enable post-transcriptional control of gene expression. Nat. Biotechnol. *22*, 841–847.

Kang, J.H., Super, M., Yung, C.W., Cooper, R.M., Domansky, K., Graveline, A.R., Mammoto, T., Berthet, J.B., Tobin, H., Cartwright, M.J., et al. (2014). An extracorporeal blood-cleansing device for sepsis therapy. Nat. Med. *20*, 1211–1216. http://dx.doi.org/10.1038/nm.3640.

Karzbrun, E., Tayar, A.M., Noireaux, V., and Bar-Ziv, R.H. (2014). Synthetic biology. Programmable on-chip DNA compartments as artificial cells. Science *345*, 829–832.

Kobayashi, H., Kaern, M., Araki, M., Chung, K., Gardner, T.S., Cantor, C.R., and Collins, J.J. (2004). Programmable cells: interfacing natural and engineered gene networks. Proc. Natl. Acad. Sci. USA *101*, 8414–8419.

Kobori, S., Ichihashi, N., Kazuta, Y., and Yomo, T. (2013). A controllable gene expression system in liposomes that includes a positive feedback loop. Mol. Biosyst. *9*, 1282–1285.

Kotula, J.W., Kerns, S.J., Shaket, L.A., Siraj, L., Collins, J.J., Way, J.C., and Silver, P.A. (2014). Programmable bacteria detect and record an environmental signal in the mammalian gut. Proc. Natl. Acad. Sci. USA *111*, 4838–4843.

Kuruma, Y., Stano, P., Ueda, T., and Luisi, P.L. (2009). A synthetic biology approach to the construction of membrane proteins in semi-synthetic minimal cells. Biochim. Biophys. Acta *1788*, 567–574.

Lucks, J.B., Qi, L., Mutalik, V.K., Wang, D., and Arkin, A.P. (2011). Versatile RNA-sensing transcriptional regulators for engineering genetic networks. Proc. Natl. Acad. Sci. USA *108*, 8617–8622.

Lutz, R., and Bujard, H. (1997). Independent and tight regulation of transcriptional units in Escherichia coli via the LacR/O, the TetR/O and AraC/I1-I2 regulatory elements. Nucleic Acids Res. *25*, 1203–1210.

Martin, V.J., Pitera, D.J., Withers, S.T., Newman, J.D., and Keasling, J.D. (2003). Engineering a mevalonate pathway in Escherichia coli for production of terpenoids. Nat. Biotechnol. *21*, 796–802.

Martinez, A.W., Phillips, S.T., Butte, M.J., and Whitesides, G.M. (2007). Patterned paper as a platform for inexpensive, low-volume, portable bioassays. Angew. Chem. Int. Ed. Engl. *46*, 1318–1320.

Mutalik, V.K., Qi, L., Guimaraes, J.C., Lucks, J.B., and Arkin, A.P. (2012). Rationally designed families of orthogonal RNA regulators of translation. Nat. Chem. Biol. *8*, 447–454.

Noireaux, V. (2013). http://www.openwetware.org/wiki/Biomolecular_Breadboards:Protocols:cost_estimate

Pardee, K., Necakov, A., and Krause, H. (2011). Nuclear receptors: small molecule sensors that coordinate growth, metabolism and reproduction. In A Handbook of Transcription Factors. Subcellular Biochemistry, *Volume 52*, First Edition, Hughes, T.R., ed. (New York: Springer), pp. 123–153.

Schmidt, J.A. (2010). Electronic spectroscopy of lignans. In Lignin and Lignans: Advances in Chemistry, C. Heitner, D. Dimmel, and J. Schmidt, eds. (Boca Raton, FL: CRC Press), pp. 49–102.

Shimizu, Y., and Ueda, T. (2010). PURE technology. Methods Mol. Biol. *607*, 11–21.

Shimizu, Y., Inoue, A., Tomari, Y., Suzuki, T., Yokogawa, T., Nishikawa, K., and Ueda, T. (2001). Cell-free translation reconstituted with purified components. Nat. Biotechnol. *19*, 751–755.

Sun, Z.Z., Yeung, E., Hayes, C.A., Noireaux, V., and Murray, R.M. (2014). Linear DNA for rapid prototyping of synthetic biological circuits in an Escherichia coli based TX-TL cell-free system. ACS Synth. Biol. *3*, 387–397.

Takahashi, M.K., Chappell, J., Hayes, C.A., Sun, Z.Z., Kim, J., Singhal, V., Spring, K.J., Al-Khabouri, S., Fall, C.P., Noireaux, V., Murray, R.M., and Lucks, J.B. (2014). Rapidly characterizing the fast dynamics of RNA genetic circuitry with cell-free transcription-translation (TX-TL) systems. ACS Synth. Biol. *March 28*, A–M. http://dx.doi.org/10.1021/sb400206c.

Takanaga, H., and Frommer, W.B. (2010). Facilitative plasma membrane transporters function during ER transit. FASEB J. *24*, 2849–2858.

Torella, J.P., Ford, T.J., Kim, S.N., Chen, A.M., Way, J.C., and Silver, P.A. (2013). Tailored fatty acid synthesis via dynamic control of fatty acid elongation. Proc. Natl. Acad. Sci. USA *110*, 11290–11295.

Yan, L., Zhou, J., Zheng, Y., Gamson, A.S., Roembke, B.T., Nakayama, S., and Sintim, H.O. (2014). Isothermal amplified detection of DNA and RNA. Mol. Biosyst. *10*, 970–1003.

Yurke, B., Turberfield, A.J., Mills, A.P., Jr., Simmel, F.C., and Neumann, J.L. (2000). A DNA-fuelled molecular machine made of DNA. Nature *406*, 605–608.

Zhang, F., Carothers, J.M., and Keasling, J.D. (2012). Design of a dynamic sensor-regulator system for production of chemicals and fuels derived from fatty acids. Nat. Biotechnol. *30*, 354–359.